

Article

Possible Role of Vesicles on Metallocatalytic Reduction Reaction of 5-Hydroxymethylfurfural to 2,5-Dimethylfuran

Toshinori Shimanouchi ^{1,*}, Yuki Takahashi ¹, Keita Hayashi ² , Kazuma Yasuhara ³ and Yukitaka Kimura ¹

¹ Graduate School of Environmental and Life Science, Okayama University, 3-1-1 Tsushimanaka, Kita-ku, Okayama 700-8530, Okayama, Japan

² Department of Chemical Engineering, Nara National College of Technology, 22 Yada-cho, Yamatokohriyama 639-1080, Nara, Japan

³ Division of Materials Science, Nara Institute of Science and Technology (NAIST), 8916-5 Takayama-cho, Ikoma 630-0192, Nara, Japan

* Correspondence: tshima@cc.okayama-u.ac.jp; Tel.: +81-86-251-8908

Abstract: A reduction reaction of 5-hydroxymethylfurfural to 2,5-dimethylfuran (2,5-DMF) has been previously performed in an organic solvent under high-temperature conditions. For the relaxation of such reaction conditions, conventional palladium on carbon (Pd/C) was combined with vesicles composed of phospholipids or surfactants. Pd/C combined with 1,2-dioleoyl-sn-glycero-3-phosphocholine indicated a yield (25%) at 60 °C compared with Pd/C (17%). Vesicles at the liquid crystalline phase were advantageous for the reduction reaction of HMF. The yield of 2,5-DMF catalyzed by Pd/C combined with the vesicles depended on the lipid composition of the vesicles. It was clarified that the yield of 2,5-DMF could be controlled by the hydration property of the vesicles. Compared with conventional 2,5-DMF synthesis in an organic solvent, the use of vesicles made it possible to reduce the burden of using organic solvents in high-temperature conditions, although limitedly.



Citation: Shimanouchi, T.; Takahashi, Y.; Hayashi, K.; Yasuhara, K.; Kimura, Y. Possible Role of Vesicles on Metallocatalytic Reduction Reaction of 5-Hydroxymethylfurfural to 2,5-Dimethylfuran. *Compounds* **2022**, *2*, 321–333. <https://doi.org/10.3390/compounds2040027>

Academic Editor: Marco Martino

Received: 6 October 2022

Accepted: 27 October 2022

Published: 3 November 2022

Publisher's Note: MDPI stays neutral with regard to jurisdictional claims in published maps and institutional affiliations.



Copyright: © 2022 by the authors. Licensee MDPI, Basel, Switzerland. This article is an open access article distributed under the terms and conditions of the Creative Commons Attribution (CC BY) license (<https://creativecommons.org/licenses/by/4.0/>).

1. Introduction

Biofuels are of great importance in the field relating to energy production using biomasses. 2,5-Dimethylfuran (2,5-DMF) is expected to be one of the promising liquid fuels obtained from biomasses and has the potential to relieve global fossil fuel shortages and air pollution problems [1]. 2,5-DMF possesses excellent energy density, boiling point, octane value, hydrophobic property, and production efficiency [1–4]. The characteristics of DMF have been thoroughly reported: engine performance and emission for DMF-based fuel, ignition delay, and combustion duration have been comprehensively evaluated so far [2]. It has been reported that 2,5-DMF can be obtained from 5-hydroxymethylfurfural (HMF), which is a compound derived from biomass [5–8]. The conventional method to obtain 2,5-DMF from HMF requires an acidic condition using aldehyde acid and sulfonic acid [6], high temperature/pressure (130 °C/0.7 MPa) [5], the use of harmful tetrahydrofuran (THF) as a solvent [9,10], and heterogeneous catalysts [5–8,11–13]. It would be difficult to consider that these reaction conditions are an environmentally benign and safe process.

2,5-DMF is yielded by a reduction reaction of HMF. The essence of the reduction/oxidation reaction, including the conversion of HMF to 2,5-DMF, is a proton transfer from substrate associated with electron transfer via metal species of catalysts. The metal-ligand complex [12], metal ion [13], or metal-supported catalysts [14] to promote proton/electron transfer have been widely studied. For example, Pd/C [6], Ru/C [15], Ru/Co₃O₄ [5], and others [8,16] have been reported to catalyze the reduction reaction of HMF to 2,5-DMF.

Recently, an improvement in a metal catalyst by phospholipid vesicles (a closed phospholipid bilayer) was reported [17–19]. One contribution is that phospholipid vesicles made

it possible to facilitate the catalytic oxidation reaction [18,19]. This is because enhanced reactivity by phospholipid vesicles (liposomes) resulted from the polarized water bound to phospholipid vesicles [17,18]. Such bound water makes it possible to enhance proton transfer from a substrate, such as cholesterol [17] and dopamine [18]. Bound water has been studied in vesicles composed of phospholipids [20] or surfactants [21,22]. Interestingly, a recent study using terahertz time-domain spectroscopy revealed bound water to phospholipid vesicles [23,24]. Water molecules strongly bind to phospholipids at the surface of phospholipid vesicles, whereas water loosely binds to bulk water [23]. Crucially, an intensification of the intermolecular binding of bound water with lipids occurs during the gel-to-rippled gel phase transition (pretransition) [24]. Another possible contribution of vesicles to enhanced reactivity is to act as a nanoscopic reaction field. Vesicles can supply the nano-sized void (free volume) in the lipid bilayer where organic compounds can be partitioned and laterally diffused [25]. Such a property has resulted in the enhanced reactivity of some reactions, including the Horner–Wadsworth–Emmons reaction [26], Aldol reaction [27], and Belousov–Zhabotinsky reaction [28]. Thus, the interior of the lipid membrane of vesicles is available for the reduction reaction of HMF in the water phase under mild temperature conditions relative to previous conditions, such as 130–260 °C [5,6,15,16].

From these paragraphs, we suppose that vesicles can contribute to the reduction reaction of HMF to 2,5-DMF. This is because HMF ($\log P_{ow} = -0.15$) favors both bulk water and organic phases and because 2,5-DMF ($\log P_{ow} = 2.24$) is present in the organic phase. It is noted that the $\log P_{ow}$ value, which is the concentration ratio of the substrate in octanol to the water phase, represents the hydrophobicity of the individual substrate. A combination of vesicles with conventional metal catalysts would improve the solvent environment for the HMF reduction reaction. Herein, we report the possible role of vesicles on the metal-supported catalyst. Then, the vesicle-combined metal-supported catalysts (VCMSCs) were prepared by using Pd/C. The potential ability to convert HMF to 2,5-DMF was examined by using VCMSCs. We investigated how vesicles worked the reduction reaction of HMF under mild temperature conditions compared with previous ones [5,6,15,16].

2. Materials and Methods

2.1. Materials

Commercially available metal-supported catalysts Pd/C were purchased from Wako Pure Chemical Co. Ltd. (Hiroshima, Japan). Four kinds of phospholipids such as 1,2-dipalmitoyl-*sn*-glycero-3-phosphocholine (DPPC; $T_m = 41.4$ °C), 1,2-dimyristoyl-*sn*-glycero-3-phosphocholine (DMPC; $T_m = 23.4$ °C), 1-palmitoyl-2-oleoyl-*sn*-glycero-3-phosphocholine (POPC; $T_m = -3$ °C), and 1,2-dioleoyl-*sn*-glycero-3-phosphocholine (DOPC; $T_m = -20$ °C) were used herein (these lipids were purchased from Wako Pure Chemical Co. Ltd., Hiroshima, Japan). In addition, sorbitan monooleate (Span 20 and 40), Tween 20, and Tween 40 were used. Chemical structures of lipids are shown in Figure 1. 5-hydroxymethylfurfural (HMF), 2,5-Dimethylfuran (2,5-DMF), 5-methyl-2-furaldehyde (MF), and 2,5-bis (hydroxymethyl) furan (BHMF) were purchased from Wako Pure Chemical Co. Ltd., Osaka, Japan. Other chemicals were of analytical grade.

2.2. Preparation of Catalyst

The desired amount of Pd/C was loaded into the batch reactor, and hydrogen gas was thereafter injected. A 2 h-incubation achieved hydrogen adsorption onto metal-supported catalysts, which led to catalytic activity. This is because no reaction was observed without the treatment of hydrogen adsorption.

2.3. Preparation of Vesicles

For phospholipid vesicles, the hydration method was performed according to a previous report [29]. The lipid mixture was dissolved in chloroform and then dried onto the wall of a round-bottom flask in vacuum and was then left overnight to ensure the removal of all of the solvent. The dried thin lipid film was hydrated with water to form multilamellar

vesicles (MLVs). Large unilamellar vesicles (LUVs) were formed from MLVs with five cycles of freeze–thaw treatment. All vesicles were treated with an extrusion method to adjust their diameter to 100 nm. Nonphospholipid vesicles composed of Span and Tween series were prepared according to the two-step emulsification method [21,22,30].

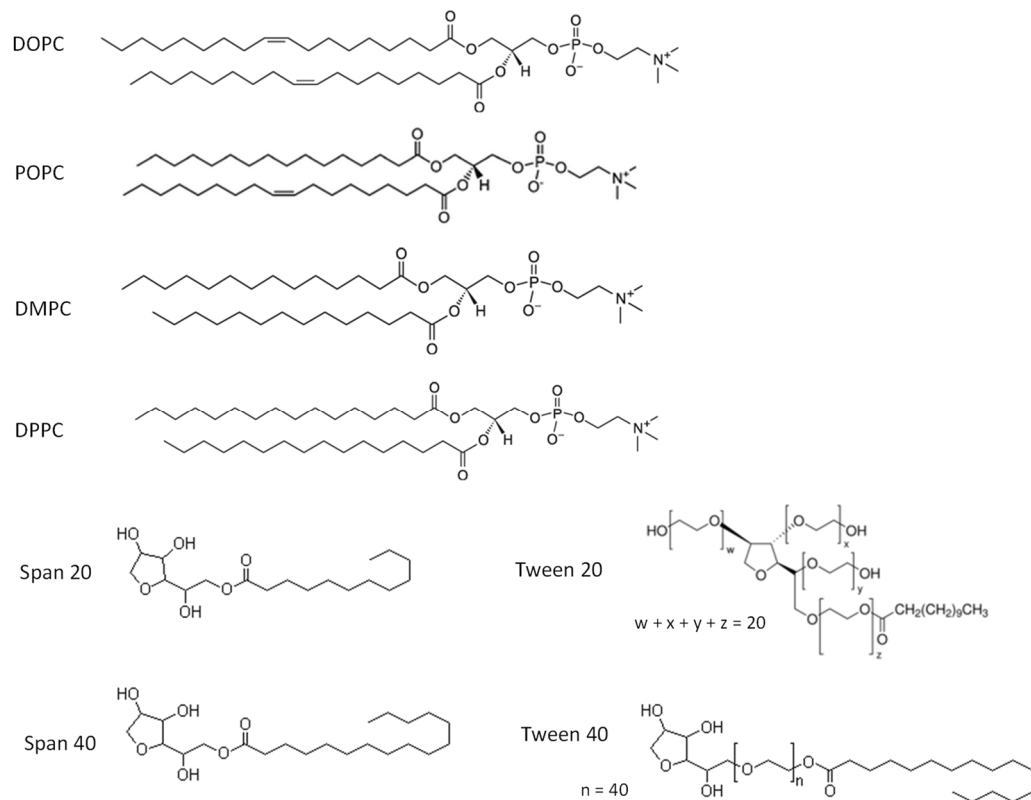


Figure 1. Chemical structure of various lipids used in this study.

2.4. Synthesis of 2,5-DMF

HMF (2.0×10^{-2} mol) was solved in 10 mL of THF, and metal-supported catalyst such as Pd/C (metal: 4.7×10^{-5} mol) was thereafter added to the solution. The reaction mixture was incubated for 6–24 h at 60 °C. To examine the effect of vesicles on the conversion of HMF to 2,5-DMF, 0.5 mL of vesicle suspension (lipids 2×10^{-6} mol) was added to 10 mL of HMF in THF solution (water content 4.7 vol%). The mixture incubated for 6–24 h was thereafter separated into liquid and solid fractions. The HMF and 2,5-DMF contents were analyzed by high-performance liquid chromatography. For a determination of HMF concentration, we used 5C18-AR-II column (NACALAI TESQUE, COSMOSIL, 4.6×150 mm) incubated at 38 °C by column oven (CO-8020, TOSO Co. Ltd., Tokyo, Japan). The flow rate of mobile phase (H₂O/MeOH = 80/20 v/v) was 1.0 mL/min, and the wavelength of UV detector (SPD-6A, Shimazu, Kyoto, Japan) was 280 nm for HMF and 234 nm for 2,5-DMF. The retention times for HMF and 2,5-DMF were 4.8 and 7.3 min, respectively. Moreover, the retention times for possible intermediates are MF, 4.70 min; BHMF, 4.70 min; furfuryl alcohol, 7.04 min; furan, 4.10 min; 2,5-diformylfuran (DFF), 6.00 min; methyl furfral, 13.7 min; and MFA, 15.2 min. The data for HMF conversion and 2,5-DMF yield were triplicated to calculate their standard error. All data are displayed as mean value \pm standard error.

2.5. Observation of Microscopic Structures

Samples contained Pd/C and vesicles (250 or 0 µM) and were incubated at room temperature for 1 h. In brief, a 5 µL aliquot of diluted solution was placed on a copper grid (400-mesh) covered with a carbon-coated collodion film for 1 min, and the excess

sample solution was removed by blotting with filter paper. After the residual solution had dried up, the grid was negatively stained with a 2% (*w/v*) phosphotungstic acid solution. Again, the liquid on the grid was removed with filter paper and dried. TEM images were acquired using a JEOL JEM-3100fef transmission microscope (JEOL, Tokyo, Japan) with an acceleration voltage of 300 kV. In the case of cryo-TEM, samples were rapidly frozen by an EM-CPC (LEICA). Other operations were similar to the conventional TEM observation.

2.6. Calcein Leakage Experiment

Calcein leakage from vesicles was evaluated according to a previous report [31]. The vesicle containing calcein (0.1 M) was prepared in a similar manner to that described above for vesicles in pure buffer solution, with the only difference being that the solution with which the lipids were hydrated was 0.1 M Tris-HCl, pH 7.5, containing 0.1 M calcein. Untrapped calcein was removed from the calcein-containing vesicles by size exclusion chromatography using a Sepharose 4B column (diameter, 1 cm; length, 15 cm; applied sample volume, 0.5 mL), 0.1 M Tris-HCl/150 mM NaCl, and pH 7.5 as elution buffer. The fluorescence intensity of the vesicles containing entrapped calcein was measured and found to be low due to self-quenching. To follow the leakage of entrapped calcein after PLC addition, the PLC solution was mixed with vesicle suspension to yield 0.1 mM lipids and 10 μ M PLC. The change in fluorescence intensity due to calcein leakage from the vesicles was monitored with an FP6500 fluorescence spectrometer from JASCO, Tokyo, Japan. Excitation and emission wavelengths were set at 490 and 520 nm, respectively. The amount of calcein leaked after time *t* was calculated according to Equation (1)

$$\text{(calcein leakage)} (\%) = 100 (I_t - I_0) / (I_{\max} - I_0) \quad (1)$$

where I_0 , I_t , and I_{\max} are the fluorescence intensities measured at the beginning of the experiment at time *t* and after addition of 3% triton X-100, respectively. The time course of calcein leakage was monitored from the mixing of vesicles with THF solution.

2.7. Dielectric Dispersion Analysis

Dielectric dispersion analysis permits to monitor the dipole moment, such as water. An RF impedance analyzer (Agilent, Santa Clara, CA, USA, 4219B; 1 MHz–1 GHz) and a network analyzer (Agilent, N5230C; 500 MHz–50 GHz) were used to monitor bulk water and water bound to vesicles. The vesicle suspension (about 30 mM for lipids) was loaded onto the electrode. We kept the sample for 30 min at constant temperature before starting measurement. Thereafter, the relative permittivity (ϵ') and dielectric loss (ϵ'') for the vesicle suspension were measured as a function of frequency and at each temperature, according to previous reports [29]. The frequency dependence of ϵ' and ϵ'' (1 MHz–50 GHz) were analyzed with the following Debye's equation:

$$\epsilon' - \epsilon'_h = \sum_{i=1}^4 \frac{\Delta\epsilon_i}{1 + (f/f_{ci})^2} \quad (2)$$

$$\epsilon'' - \frac{G_{dc}}{2\pi f C_0} = \sum_{i=1}^4 \frac{\Delta\epsilon_i(f/f_{ci})}{1 + (f/f_{ci})^2} \quad (3)$$

where ϵ'_h and G_{dc} mean the limit of relative permittivity at higher frequency and direct current conductivity of vesicle suspensions. C_0 is the cell constant obtained by a calibration using water, methanol, and ethanol in the frequency range 1 MHz to 1 GHz. Alternatively, a calibration was carefully performed by using distilled water in the range 500 MHz to 50 GHz.

It has been reported that vesicle suspension has three different characteristic relaxations: the lateral diffusion of ionic species (*i* = 1, first step, several MHz); the rotational Brownian motion of lipid headgroups (*i* = 2, second step, 20–50 MHz; L_r) [29]; the water bound to vesicle membranes (*i* = 3; third step, 200–500 MHz; W_L) [18,22,32], and (iv) free

water ($i = 4$; fourth step, 20–30 GHz) [18,22,32]. Therefore, Equations (2) and (3) were assumed to be written by a summation of three relaxation terms.

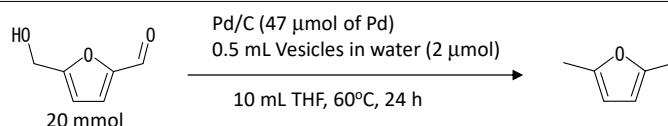
3. Results and Discussion

3.1. Characterization of Metal Catalyst Combined with Vesicles

We focused on the development of vesicle-combined metal-supported catalysts (VCMSCs) to function in THF as the reaction solvent for 2,5-DMF synthesis via an HMF reduction reaction. In the first series of experiments, the VCMSCs were then characterized. Generally, THF has an impact on vesicle stability, although THF has recently been used as a size adjustor in the case of vesicle preparation by homopolymer [33]. A cryo-TEM image for phospholipid vesicles prepared by DOPC is shown in Figure 2a. Overall, DOPC vesicles were unilamellar, and their mean diameter was 110.2 nm (determined by more than 100 vesicles observed in cryo-TEM images), which was in agreement with the result obtained by a dynamic light scattering measurement (105.4 nm). The mixture of DOPC vesicle suspension with THF solution was also observed with cryo-TEM. Some emulsion-like images were confirmed (arrows in Figure 2b). Interestingly, some vesicles kept themselves without any disruption. The fraction of vesicle disruption should be quantified with adequate methods other than cyro-TEM observation. This is because a quantification using cryo-TEM observation easily involves statistical uncertainty. Then, the fraction of vesicle disruption was quantified with a probe leakage experiment [21,31,34]. Calcein was thereby used here since calcein can be easily encapsulated in vesicles, and calcein leakage is then well known as the typical index for the stability of vesicle membranous structures [34]. Thereby, various vesicles encapsulating calcein were mixed with THF to investigate calcein leakage. More than 60% of the calcein leakage for DOPC vesicles was observed independent of the water content to THF (X_W) (Figure 2c). The calcein leakage at $X_W = 4.7$ vol% was unlikely to depend on the kinds of lipids, as shown in Figure 2d. Every vesicle had 50% calcein leakage or more, indicating obviously that many vesicles were ruptured, although a part of the vesicles might remain in keeping their structure, which is consistent with the direct observations with cryo-TEM (Figure 2b).

Table 1. Additive effect of vesicles on HMF conversion and 2,5-DMF yield.

Entry	Composition *	Water Content [vol%]	HMF Conversion # [%]	2,5-DMF Yield # [%]
1	None	0	54.3 ± 2.3	17.1 ± 1.7
2	DOPC	4.7	41.2 ± 2.9	25.3 ± 2.6
3	POPC	4.7	55.2 ± 2.5	12.1 ± 2.9
4	DMPC	4.7	0	0
5	DPPC	4.7	0	0
6	Span40/Tween40(50/50)	4.7	55.5 ± 2.6	0
7	Span40/Tween40(75/25)	4.7	55.5 ± 3.2	5.2 ± 1.3
8	Span20/Tween20(50/50)	4.7	64.2 ± 2.9	0.8 ± 0.2
9	Span20/Tween20(75/25)	4.7	61.7 ± 2.2	7.2 ± 1.8



* Value in parenthesis is the molar ratio; # HMF conversion and 2,5-DMF yield were calculated from HPLC data shown in Figure 3a. All the experiments were triplicated, and the mean value ± standard error is displayed.

Next, we confirmed the vesicle structure in the presence of Pd-supported carbon black (Pd/C) in water by cryo-TEM observation. Overall, spherical Pd/C catalysts were observed (Figure 2e). Their diameter distribution was analyzed to calculate the mean diameter (~685 nm), as shown in Figure 2f. Thereafter, the Pd/C catalyst was combined with DOPC vesicles (entry 2). As shown in Figure 2g, some vesicles were observed neighboring the Pd/C surface in the THF solvent. It is noted that emulsion-like droplets

observed in Figure 2b were unlikely to be present at the surface of Pd/C. Pd/C combined with DOPC vesicles was complementarily observed with the negative staining method. Some vesicles were observed at the surface of Pd/C (Figure 2h). Bearing in mind that TEM observations should be performed in a vacuum, DOPC vesicles were successfully combined, even in the THF solvent, with Pd/C retaining its own bilayer structure.

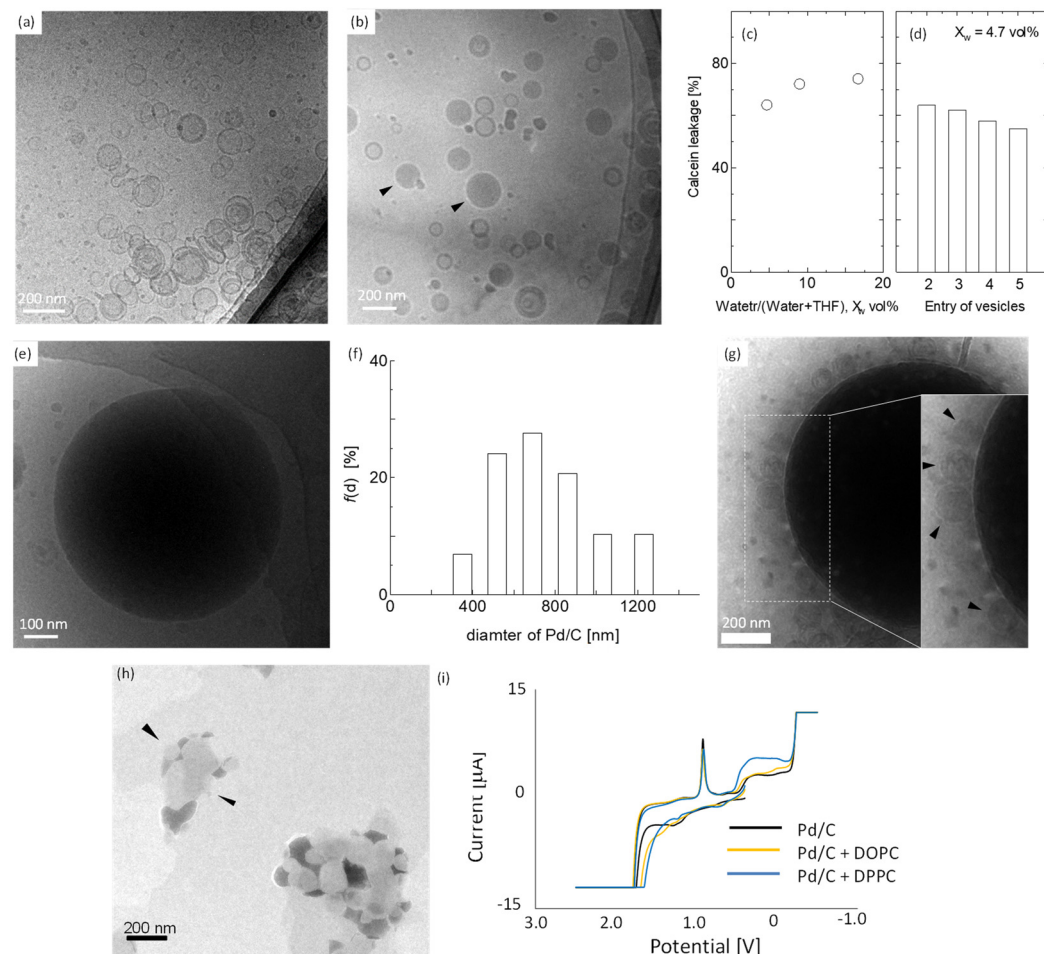


Figure 2. Characterization of the vesicle-combined metal-supported catalyst using DOPC vesicles and Pd/C. Cryo-TEM images of DOPC vesicles in the (a) absence and (b) presence of THF. Arrows: typical example of emulsions. (c) Relationship between calcine leakage from DOPC vesicle (entry 2) and water content in THF. Calcine leakage was obtained 24 h later after the injection of vesicles encapsulating calcine. (d) Calcine leakage from various types of vesicles at $X_w = 4.7$ vol%. Entry numbers are listed in Table 1. (e) Cryo-TEM image of Pd/C and (f) a diameter distribution of Pd/C. (g) Cryo-TEM and (h) TEM image of Pd/C in the presence of DOPC vesicles. Samples were stained by phosphate tungsten acid at the TEM observation. (i) Cyclic voltammogram for Pd/C in the absence and presence of vesicles. DOPC and DPPC vesicles (100 nm), supported electrolytes: 0.5 M H_2SO_4 . Working electrode: Pt; counter electrode: Pt; reference electrode: Ag/AgCl; scan rate (positive), 0.01/s; initial voltage, 0.4 V; high potential, 2.5 V; low potential, 0.5 V.

It is an electrochemical property of VCMSCs and Pd/C that determines the catalytic reactivity to 2,5-DMF synthesis. Whether the complexation of vesicles affected the electrochemical property of Pd/C was examined with the cyclic voltammogram method. A cyclic voltammogram can evaluate the reduction–oxidation potential that relates to the property of the electron transfer of metal, which is the index of catalytic activity. The complexation of DOPC (entry 2) and DPPC (entry 5) to the suspension of Pd/C resulted in no alteration in the cyclic voltammogram, as shown in Figure 2i, suggesting no influence of the vesicles

on the electrochemical property of Pd/C. The same was true for other types of vesicles (entries 3,4,6–9) (data not shown).

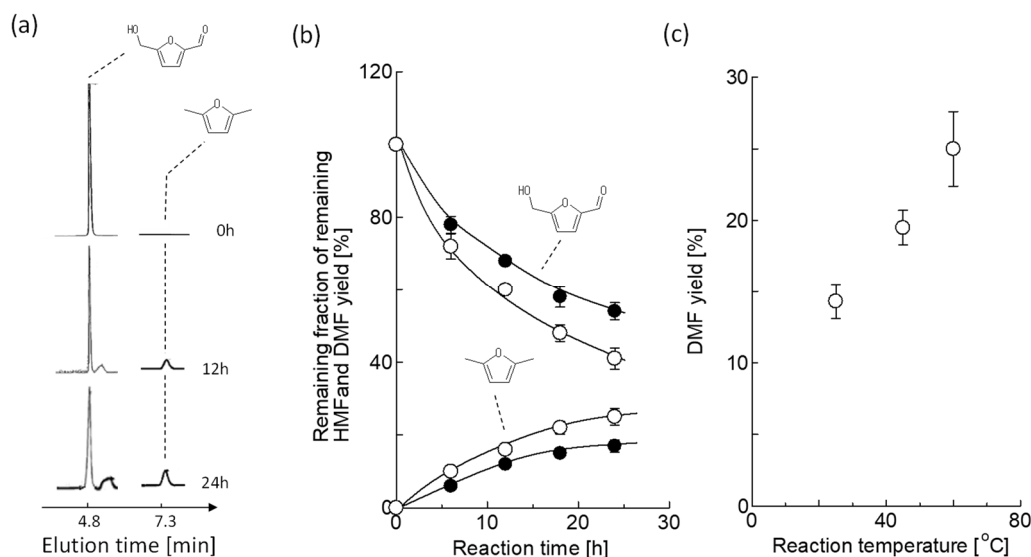


Figure 3. Time course of HMF conversion: (a) HPLC data, HMF (280 nm) and DMF (234 nm); (b) HMF yield and 2,5-DMF yield; closed key, Pd/C (entry 1); open key, VCMSC using DOPC vesicles (entry 2); the reaction temperature, 60 °C; (c) temperature effect on DMF yield obtained by VCMSC using DOPC. All the experiments were triplicated, and the mean values \pm standard errors are shown.

From this characterization of the VCMSCs, their use in 2,5-DMF synthesis was expected as well as bare Pd/C.

3.2. 2,5-DMF Synthesis by VCMSCs

Previously, the conversion of HMF to 2,5-DMF was conducted by Pd/C under 130 °C [5,9,10]. However, VCMSCs using vesicles cannot be applied to this temperature condition because of low thermal stability [34]. Then, the reaction temperature was herein selected to be 60 °C as the present reaction condition. The reasons were (i) the boiling point of THF is 65 °C and (ii) the thermal stability of vesicles as supramolecular assemblies. Figure 3a shows the HPLC data at 0 to 24 h. The peaks were detected at 4.8 min for the remaining HMF and 7.3 min for the produced 2,5-DMF, although unknown peaks at 5.8–6 min were detected. Figure 3b shows the time course of the remaining HMF and 2,5-DMF yield obtained from Figure 3a. The addition of VCMSC relative to Pd/C resulted in a significant decrease in the remaining HMF (54.3 \pm 2.3 to 41.2 \pm 2.9%) and an increase in 2,5-DMF yield (17.1 \pm 1.7 to 25.3 \pm 2.6%). To clarify the additive effect of vesicles, the aliquot of water equivalent to vesicle suspension was added to the reaction system. The resulting yield of 2,5-DMF was similar to that for Pd/C alone (data not shown). From the result, the VCMSC-catalyzed production of 2,5-DMF was likely to originate from the vesicle, not from water. Next, the optimal temperature condition to expect the vesicles without any disruption due to a thermal effect was roughly screened, as shown in Figure 3c. A temperature condition of 60 °C was optimal in the present work.

The effect of VCMSCs using other vesicles on the conversion of HMF to 2,5-DMF was investigated at 60 °C. A total of 0.5 mL of vesicle suspension was added to the reaction system, including 0.2 mM of Pd/C as the final lipid concentration, and the reaction temperature was 60 °C. The yield of 2,5-DMF depended on the lipid composition, whereas no large alteration in the conversion of HMF was observed (Table 1). The order of the 2,5-DMF yield was DPPC~DMPC < POPC < DOPC (entries 2–5), and the yield of 2,5-DMF in the presence of DOPC vesicles was comparable with that in the absence of vesicles (entry 1). Furthermore, the above order of vesicles in the 2,5-DMF yield corresponded with the order for either the membrane fluidity [29] or hydration property [17,18,20] of

vesicles. Likewise, the effect of VCMSCs using nonphospholipid vesicles on the conversion of HMF to 2,5-DMF was examined. Span20/Tween20 and Span40/Tween40 vesicles are fluid vesicles possessing bound water as compared with vesicles [21,22]. Overall, the 2,5-DMF yield was in the range of 0 to $7.2 \pm 1.8\%$ (Table 1, entries 6–9). Comparing entries 6 with 7 and entries 8 with 9, the increase in the molar ratio of Span40 and Span20 elevated the 2,5-DMF yield: 0 to $5.2 \pm 1.3\%$ and 0.8 ± 0.2 to $7.2 \pm 1.8\%$, respectively.

Bearing in mind that vesicles possess much more polarized bound water than Span/Tween vesicles [18,21,22,29] and that an increase in the Span content in vesicles affords hydration and membrane fluidity [22], the dependency of the lipid composition in VCMSCs on reactivity (Table 1) suggested that the polarized bound water was likely to contribute to the reaction process of HMF to 2,5-DMF. Thereby, the contribution of polarized bound water to the reduction reaction of HMF to 2,5-DMF was examined by the solvent isotope effect. DOPC vesicles prepared in D_2O were used to prepare VCMSCs. A definite reduction in the 2,5-DMF yield was observed. No conversion of HMF in D_2O indicated that the H_2O -induced products were not the precursor of 2,5-DMF.

3.3. Relationship between Hydration Property of Vesicles and Reactivity

Vesicles generally possess bound water [17,20–22,32], which is one of the dominant factors for the hydration property of vesicles. In the case of vesicles, water mainly binds to the phosphorous ester group (PO_2^-). Therefore, bound water can be estimated by the peak shift in the asymmetry stretching vibration of PO_2^- (observed at around 1240 cm^{-1}) in an FTIR measurement. In addition, dielectric measurements can give qualitative and quantitative information with respect to bound water to vesicles [12,18,33]. Both measurements are well comparable with each other, and we investigated the hydration property of vesicles by using the dielectric measurement because Span40 and Span60 have no PO_2^- group.

Figure 4a shows the typical dielectric spectra (between 1 MHz and 1 GHz) for DOPC (entry 2) and DPPC (entry 5) vesicles at 39 mM of lipid concentration C_{lip} . The spectra had characteristic relaxations attributed to the rotational Brownian motion of phospholipid headgroups (20~50 MHz; L_r) and bound water to vesicles (200~500 MHz; W_L). The spectra were then analyzed to evaluate the amplitude of the dielectric relaxation $\Delta\epsilon_{\text{hyd}}$ observed at the range of W_L based on previous reports [18,32]. The $\Delta\epsilon_{\text{hyd}}$ values for DOPC and DPPC vesicles were 4.8 and 0.7, respectively. According to the classic Debye's theorem in liquid physics, the $\Delta\epsilon_{\text{hyd}}$ value is theoretically proportional to the term (the number of bound water to lipids) × (the polarizability of bound water) [20]. To take into consideration the contribution of the amount of bound water to lipids, $\Delta\epsilon_{\text{hyd}}/C_{\text{lip}}$ was plotted against the C_{lip} value (Figure 4b). Rough linearity of $\Delta\epsilon_{\text{hyd}}/C_{\text{lip}}$ to C_{lip} was observed in the case of DOPC ($r^2 = 0.90$) and DPPC ($r^2 = 0.92$). The same was true for other lipids (data not shown). Then, we defined the slope of $\Delta\epsilon_{\text{hyd}}/C_{\text{lip}}$, with $\Delta\epsilon_{\text{hyd}}/C_{\text{lip}}$ as the hydration index. The liposome membrane with a higher $\Delta\epsilon_{\text{hyd}}/C_{\text{lip}}$ value was better hydrated. The $\Delta\epsilon_{\text{hyd}}/C_{\text{lip}}$ values for various vesicles are shown in Figure 4c. In the case of phospholipids (entries 2–5), bound water was present around the PO_2^- group [35], implying the same polarizability of bound water. The resulting $\Delta\epsilon_{\text{hyd}}/C_{\text{lip}}$ value should correspond to the number of bound water molecules per lipid molecule. The DOPC vesicle (entry 2) had the strongest hydration property of the vesicles used here. In contrast, the DPPC vesicle (entry 5) had the weakest hydration property of vesicles. These trends are in agreement with previous reports [18]. It is noted that the replacement of H_2O by D_2O resulted in a definite reduction in the $\Delta\epsilon_{\text{hyd}}/C_{\text{lip}}$ value (entry 2'), which is consistent with the finding that D_2O has weaker polarizability than H_2O [36]. It was therefore considered that the index $\Delta\epsilon_{\text{hyd}}/C_{\text{lip}}$ included not only the number of bound water molecules but also its polarizability. For nonphospholipid vesicles (entries 6–9), the $\Delta\epsilon_{\text{hyd}}/C_{\text{lip}}$ value was comparable to those for the vesicles (entries 3–5), as shown in Figure 4c. The rise in the Span content of vesicles resulted in an elevation in the $\Delta\epsilon_{\text{hyd}}/C_{\text{lip}}$ value (see entries 7 to 6 and 9 to 8). It was likely that bound water was present around the sorbitol group (see chemical structures in Figure 1) [21]. It has also been reported that these vesicles were

much more hydrated compared with vesicles [21,22]. It was therefore considered that the $\Delta\epsilon_{hyd}/C_{lip}$ values for entries 6–9 were determined by the balance of the above two factors. Thus, it is reasonable that the $\Delta\epsilon_{hyd}/C_{lip}$ value is the index representing the number of bound water molecules and their polarizability.

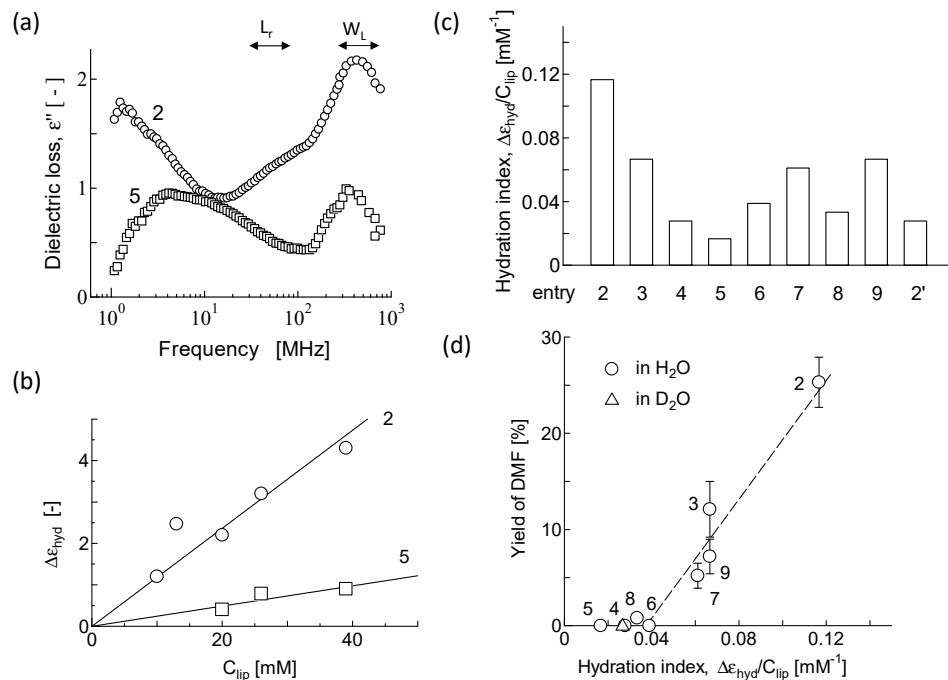


Figure 4. (a) Typical spectra for vesicles. Lipid concentration was 39 mM: L_r , the rotational Brownian motion of headgroup for lipids; W_L , bound water to lipids. (b) Relationship between the amplitude and lipid concentration. Correlation coefficients for entries 2 and 5 were $r^2 = 0.90$ and 0.92, respectively. (c) Hydration index for various vesicles. Entry numbers are listed in Table 1. Entry 2' represents DOPC in D₂O. (d) Relationship between hydration property of vesicles and their reactivity. 2,5-DMF was obtained from Pd/C-catalyzed reaction of HMF in the presence of vesicles. Entry numbers are listed in Table 1. Triangle (entry 2') represents DOPC in D₂O.

As stated in Section 3.1, some vesicles kept their own bilayer structure even in the THF solvent. It was considered that the hydration property for the vesicles should have an impact on the yield of 2,5-DMF catalyzed by VCMSCs. Then, the yield of 2,5-DMF in the presence of the respective vesicle (Table 1) was plotted against the corresponding hydration index (Figure 4c). As shown in Figure 4d, both were roughly correlated with a range of $\Delta\epsilon_{hyd}/C_{lip} > 0.04$. The range $\Delta\epsilon_{hyd}/C_{lip} < 0.04$ resulted in no 2,5-DMF yield. A comparison of DOPC in H₂O (entry 2) with DOPC in D₂O (entry 2') indicated the contribution of the polarizability of bound water to the yield of 2,5-DMF.

3.4. Possible Reaction Mechanism and Contribution of Vesicles Used in VCMSCs

As described in the last section, the 2,5-DMF yield depended on the bound water to vesicles. Then, we discussed the possible role of vesicles in VCMSCs from the aspects of the reaction mechanism of HMF to 2,5-DMF. It has been reported that the possible reaction route of HMF to 2,5-DMF is through MF-routed and BHMF-routed reactions [8], as shown in Figure 5a. The possible reaction route was herein discussed. First, both MF and BHMF could not be detected in our measurements (data not shown). In addition, in another report [8], the concentration levels of MF and BHMF were quite low at the intermediate level (by 0.1 times) [8]. Both MF and BHMF were then used as the initial substrate for DMF synthesis to determine the possible reaction route to 2,5-DMF. Figure 5b demonstrated that MF indicated a higher DMF yield than BHMF, suggesting that MF rather than BHMF was a possible intermediate for 2,5-DMF synthesis catalyzed by Pd/C and VCMSC. Previous

research [3–5,8] has revealed that the reaction of MF-routed 2,5-DMF requires (i) the supply of proton to the hydroxyl group, (ii) the hydrogen adduct by reduction catalysis in the aldehyde group, and (iii) the dehydration of two water molecules. Therefore, factors (i) to (iii) are discussed below.

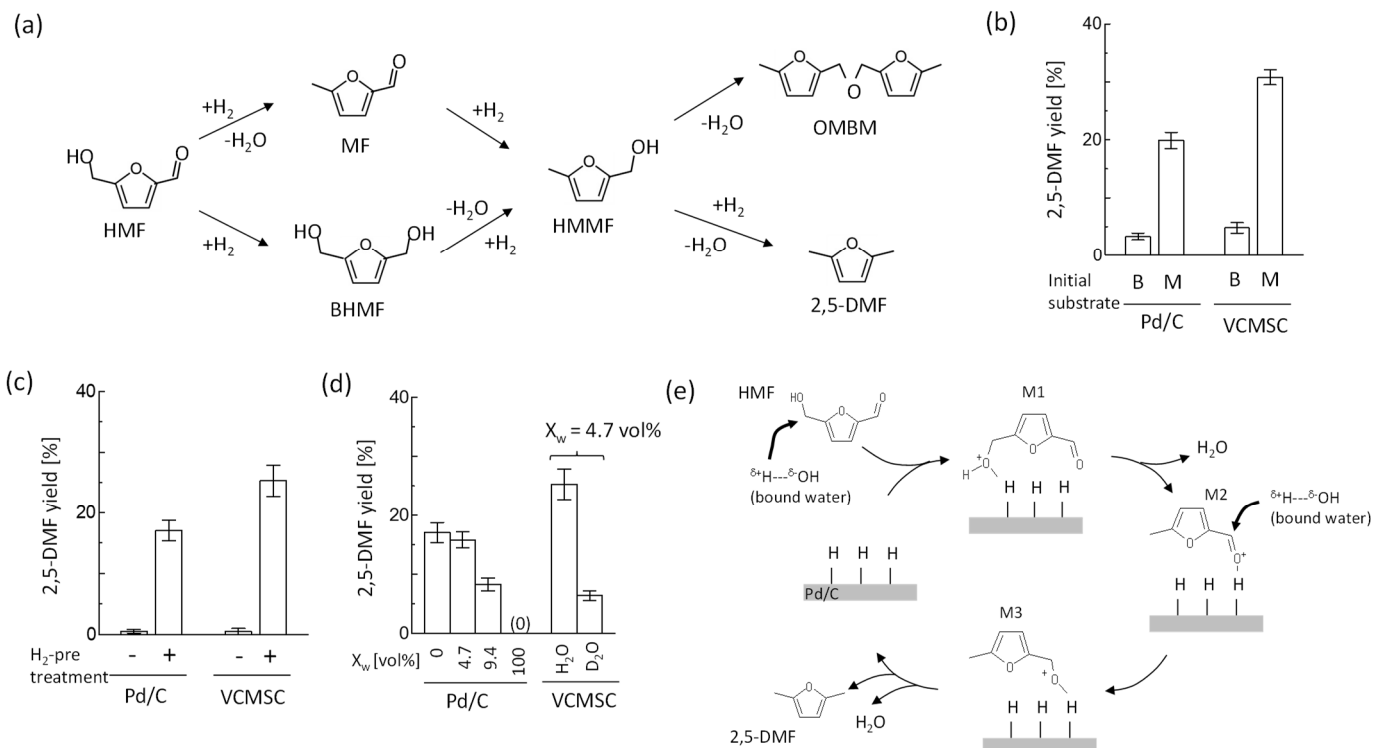


Figure 5. (a) Reaction route of HMF to 2,5-DMF. (b) Effect of initial substrate on 2,5-DMF yield: B, BHMF; M, MF. (c) 2,5-DMF yield with and without H_2 pre-adsorption treatment to Pd/C. (d) Effect of H_2O on catalytic activity of Pd/C and D_2O solvent isotope effect on DMF yield. VCMSC was Pd/C combined with DOPC vesicles. Reaction conditions: 60 °C and 24 h. (e) Possible reaction mechanism of HMF conversion to 2,5-DMF. Bound water to vesicles might contribute to the formation of intermediate M1 and M3. All the experiments were triplicated, and the mean values ± standard errors are shown.

For (i) and (ii), the effect of H_2 pretreatment on DMF yield was examined, as shown in Figure 5c. When Pd/C was pretreated in advance by H_2 , significant DMF yields were observed in the presence of Pd/C ($17.1 \pm 1.7\%$) and VCMSC ($25.3 \pm 2.6\%$). In contrast, a trace of DMF was detected without H_2 pretreatment. Therefore, the supply of a proton to the hydroxyl group was performed by hydrogen adsorbed on Pd/C (bare Pd/C and VCMSC). Moreover, the additive effect of water on 2,5-DMF was examined by altering the volume fraction of H_2O to THF. The diminished yield of 2,5-DMF was observed at $X_w = 100\%$ (Figure 5d), suggesting that bulk water definitely weakened the action of hydrogen absorbed on Pd/C. Next, the impact of the polarizability of bound water on 2,5-DMF was examined based on the D_2O solvent isotope effect because D_2O has weaker polarizability than H_2O . A definitely reduced yield of 2,5-DMF was observed in the case of VSMSC prepared by DOPC vesicles in D_2O (Figure 5d). That is, replacing bound water bearing strong polarizability (H_2O) with one with weak polarizability (D_2O) reduced the reduction reaction of HMF to DMF. Generally, the polarizability of water molecules indicates the following order: bound $\text{D}_2\text{O} <$ bound H_2O , and bulk $\text{D}_2\text{O} <$ bulk $\text{H}_2\text{O} <$ bound H_2O . Therefore, the results of Figure 5c,d suggested the contribution of bound water to vesicles, rather than bulk water, on the reduction reaction of HMF.

For (iii), phospholipid vesicles and non-phospholipid vesicles favor the partition of 2,5-DMF into the membrane interior (data not shown). The hydrophobic environment

of membrane interiors is likely to be advantageous for step (iii): the dehydration of two water molecules from HMF. Therefore, the configuration of vesicles on Pd/C similar to Figure 2g,h would be advantageous for step (iii). Moreover, the localization of vesicles on Pd/C might contribute to keeping bulk water away from bound water and not only to supplying bound water close to the reaction site.

In addition, bearing in mind the results shown in Figure 5b–d, it is considered that the reduction in HMF proceeded through cooperation between Pd/C and the vesicle (or vesicle-derived lipids), as proposed in Figure 5e. In the first step, the binding of HMF to a complex of Pd/C with vesicles (lipids) occurs. The bound water of lipids could supply hydrogen to HMF instead of hydrogen adsorbed on Pd/C. Afterward, the hydrogen on Pd/C attacks HMF to dehydrate and form M2 (equivalent to an intermediate MF). Taking into consideration that there is no yield of 2,5-DMF in DOPC/D₂O, the attack by bound water might contribute to the reaction from M2 to M3. The hydroxyl group of M3 was dehydrated to form 2,5-DMF in a similar manner to the mechanism at the beginning of reaction. Thus, it was suggested that the bound water localized close to the reaction site contributed to the reduction reaction of HMF to 2,5-DMF.

4. Conclusions

In this study, we examined the possible role of vesicles on the reduction reaction of HMF to 2,5-DMF, by combining Pd/C with vesicles. The yield of 2,5-DMF catalyzed by VCMSCs at 60 °C could achieve a mild reaction condition (conventionally 130 °C) and surpass reactivity (25.3 ± 2.6%) relative to that for Pd/C (17.1 ± 1.7%). The role of vesicles was likely to assist the proton transfer between the reaction site on Pd/C and the substrate. The action of molecular hydrogen on the reaction site of Pd/C was easily weakened by bulk water. The control of proton transfer over the reduction reaction of HMF was likely to require the localization of polarized bound water around the reaction site of Pd/C. These possible actions by vesicles made it possible to reduce the amount of organic solvent and temperature, although limitedly.

Author Contributions: Writing—original draft preparation, T.S. and Y.K.; Conducting experiments, Y.T. and T.S.; Analysis, T.S., Y.T., K.H. and K.Y. All authors have read and agreed to the published version of the manuscript.

Funding: This research was funded by The Yakumo Foundation for Environmental Science in 2016. This research was also supported by A-STEP (Japan Science and Technology Agency) in 2014. The authors thank Sakiko Fujita for her technical support in acquiring TEM and cryo-TEM images, which is part of Project: Nanotech Platform (no. NPS15046). We are also grateful to the Special Project from MEXT for the Environmental and Life Scientific Research on the Integration of Low-Carbon Society and Ensuring Food Safety and Security for financial support.

Institutional Review Board Statement: Not applicable.

Informed Consent Statement: Not applicable.

Data Availability Statement: Not applicable.

Conflicts of Interest: The authors declare no conflict of interest.

References

1. Qian, Y.; Zhu, L.; Wang, Y.; Lu, X. Recent progress in the development of biofuel 2,5-dimethylfuran. *Renew. Sustain. Energy Rev.* **2015**, *41*, 633–646. [[CrossRef](#)]
2. Hoang, A.T.; Ölcer, A.I.; Nižetić, S. Prospective review on the application of biofuel 2,5-dimethylfuran to diesel engine. *J. Energy Inst.* **2021**, *94*, 360–386. [[CrossRef](#)]
3. Gupta, N.K.; Nishimura, S.; Takagaki, A.; Ebitani, K. Hydrotalcite-supported gold-nanoparticle-catalyzed highly efficient base-free aqueous oxidation of 5-hydroxymethylfurfural into 2,5-furandicarboxylic acid under atmospheric oxygen pressure. *Green Chem.* **2011**, *13*, 824–827. [[CrossRef](#)]
4. Lange, J.P.; van der Heide, E.; van Buijtenen, J. Furfural—A Promising Platform for Lignocellulosic Biofuels. *ChemSusChem* **2012**, *5*, 150–166. [[CrossRef](#)]

5. Zu, Y.; Yang, P.; Wang, J.; Liu, X.; Ren, J.; Lu, G.; Yang, Y. Efficient production of the liquid fuel 2,5-dimethylfuran from 5-hydroxymethylfurfural over Ru/Co₃O₄ catalyst. *Appl. Cat. B Environ.* **2014**, *146*, 244–248. [[CrossRef](#)]
6. Thanananthanachon, T.; Rauychfuss, T.B. Efficient production of the liquid fuel 2,5-dimethylfuran from fructose using formic acid as a reagent. *Angew. Chem. Int. Ed.* **2010**, *49*, 6616–6618. [[CrossRef](#)]
7. Hu, L.; Zhao, G.; Hao, W.; Tang, X.; Sun, Y.; Lin, L.; Liu, S. Catalytic conversion of biomass-derived carbohydrates into fuels and chemicals via furanic aldehydes. *RSC Adv.* **2012**, *2*, 11184–11206. [[CrossRef](#)]
8. Chen, S.; Ciotonea, C.; Vigier, K.d.; Jerome, F.; Wojcieszak, R.; Dumeignil, F.; Marceau, E.; Toyer, S. Hydroconversion of 5-hydroxymethylfurfural to 2,5-dimethylfuran and 2,5-dimethyltetrahydrofuran over non-promoted Ni/SBA-15. *ChemCatChem* **2020**, *12*, 2050–2059. [[CrossRef](#)]
9. Malley, L.A.; Christoph, G.R.; Stadler, J.C.; Hansen, J.F.; Biesemeier, J.A.; Jasti, S.L. Acute and subchronic neurotoxicological evaluation of tetrahydrofuran by inhalation in rats. *Drug Chem. Toxicol.* **2001**, *24*, 201–219. [[CrossRef](#)]
10. Hermida, S.A.; Possari, E.P.; Souza, D.B.; Campos, I.D.; Gomes, O.F.; di Mascio, P.; Medeiros, M.H.; Loureiro, A.P. 20-Deoxyguanosine, 20-deoxycytidine, and 20-deoxyadenosine adducts resulting from the reaction of tetrahydrofuran with DNA bases. *Chem. Res. Toxicol.* **2006**, *19*, 927–936. [[CrossRef](#)]
11. Wang, H.; Zhu, C.; Li, D.; Liu, Q.; Tan, J.; Wang, C.; Cai, C.; Ma, L. Recent advances in catalytic conversion of biomass to 5-hydroxymethylfurfural and 2,5-dimethylfuran. *Energy Rev.* **2019**, *103*, 227–247. [[CrossRef](#)]
12. Opazo, C.; Huang, X.; Cherny, R.A.; Moir, R.D.; Roher, A.E.; White, A.R.; Cappai, R.; Masters, C.L.; Tanzi, R.E.; Inestosa, N.C.; et al. Metalloenzyme-like activity of Alzheimer’s disease-amyloid. *J. Biol. Chem.* **2002**, *277*, 40302–40308. [[CrossRef](#)] [[PubMed](#)]
13. Gentry, E.C.; Knowles, R.R. Synthetic applications of proton-coupled electrontransfer. *Acc. Chem. Res.* **2016**, *49*, 1546–1556. [[CrossRef](#)]
14. Davis, S.E.; Zope, B.N.; Davis, R.J. On the mechanism of selective oxidation of 5-hydroxymethylfurfural to 2,5-furandicarboxylic acid over supported Pt and Au catalysts. *Green Chem.* **2012**, *14*, 143–147. [[CrossRef](#)]
15. Zhang, J.H.; Lin, L.; Liu, S.J. Efficient Production of Furan Derivatives from a Sugar Mixture by Catalytic Process. *Energy Fuels* **2012**, *26*, 4560–4567. [[CrossRef](#)]
16. Yang, Y.; Liu, Q.; Li, D.; Tan, J.; Zhang, Q.; Wang, C.; Ma, L. Selective hydrodeoxygenation of 5-hydroxymethylfurfural to 2,5-dimethylfuran on Ru–MoO_x/C catalysts. *RSC Adv.* **2017**, *7*, 16311–16318. [[CrossRef](#)]
17. Shimanouchi, T.; Tasaki, M.; Vu, H.T.; Ishii, H.; Yoshimoto, N.; Umakoshi, H. Aβ/Cu-oxidation of cholesterol on liposome membrane. *J. Biosci. Bioeng.* **2009**, *109*, 145–148. [[CrossRef](#)]
18. Vu, H.T.; Shimanouchi, T.; Ishikawa, D.; Matsumoto, T.; Yagi, H.; Goto, Y.; Umakoshi, H.; Kuboi, R. Effect of liposome membranes on disaggregation of amyloid β fibrils by dopamine. *Biochem. Eng. J.* **2013**, *71*, 118–126. [[CrossRef](#)]
19. Nagami, H.; Yoshimoto, N.; Umakoshi, H.; Shimanouchi, T.; Kuboi, R. Liposome-assisted activity of superoxide dismutase under oxidative stress. *J. Biosci. Bioeng.* **2005**, *99*, 423–428. [[CrossRef](#)]
20. Bach, D.; Wachtel, E. Phospholipid/cholesterol model membranes: Formation of cholesterol crystallites. *Biochim. Biophys. Acta* **2003**, *1610*, 187–197. [[CrossRef](#)]
21. Hayashi, K.; Shimanouchi, T.; Kato, K.; Miyazaki, T.; Nakamura, A.; Umakoshi, H. Fluid, Flexible, and “Wet” Surface of Span80 Vesicle, Compared with Phospholipid Liposomes. *Colloids Surf. B* **2011**, *87*, 28–35. [[CrossRef](#)] [[PubMed](#)]
22. Hayashi, K.; Iwai, H.; Shimanouchi, T.; Umakoshi, H.; Iwasaki, T.; Kato, A.; Nakamura, H. Formation of Lens-like Vesicles Induced via Microphase Separation on a Sorbitan Monoester Membrane with Different Headgroups. *Colloids Surf. B* **2015**, *135*, 235–242. [[CrossRef](#)] [[PubMed](#)]
23. Kadomura, Y.; Yamamoto, N.; Tominaga, K. Broadband dielectric spectroscopy from sub GHz to THz of hydrated lipid bilayer of DMPC. *Eur. Phys. J. E* **2019**, *42*, 139. [[CrossRef](#)] [[PubMed](#)]
24. Penkov, N.V.; Yashin, V.A.; Belosludtsev, K.N. Hydration Shells of DPPC Liposomes from the Point of View of Terahertz Time-Domain Spectroscopy. *Appl. Spectrosc.* **2021**, *75*, 189–198. [[CrossRef](#)]
25. Gironi, B.; Lapini, A.; Ragnoni, E.; Calvagna, C.; Paolantoni, M.; Morresi, A.; Sassi, P. Free volume and dynamics in a lipid bilayer. *Phys. Chem. Chem. Phys.* **2019**, *41*, 23169–23178. [[CrossRef](#)]
26. Shimanouchi, T.; Kitagawa, Y.; Kimura, Y. Application of liposome membrane as the reaction field: A case study using the Horner–Wadsworth–Emmons reaction. *J. Biosci. Bioeng.* **2019**, *128*, 198–202. [[CrossRef](#)]
27. Hirose, M.; Fujiwara, S.; Ishigami, T.; Suga, K.; Okamoto, Y.; Umakoshi, H. Liposome Membranes Assist the l-Proline-catalyzed Aldol Reaction of Acetone and p-Nitrobenzaldehyde in Water. *Chem. Lett.* **2018**, *47*, 931–934. [[CrossRef](#)]
28. Chern, M.S.; Watanabe, N.; Suga, K.; Okamoto, Y.; Umakoshi, H. Modulation of the Belousov–Zhabotinsky Reaction with Lipid Bilayers: Effects of Lipid Head Groups and Membrane Properties. *Langmuir* **2021**, *37*, 6811–6818. [[CrossRef](#)]
29. Shimanouchi, T.; Sasaki, M.; Hiroiwa, A.; Yoshimoto, N.; Miyagawa, K.; Umakoshi, H.; Kuboi, R. Relationship between the mobility of phosphocholine headgroups of liposomes and the hydrophobicity at the membrane interface: A characterization with spectrophotometric measurements. *Colloids Surf. B* **2011**, *88*, 221–230. [[CrossRef](#)]
30. Kato, K.; Walde, P.; Koine, N.; Ichikawa, S.; Ishikawa, T.; Nagahama, R.; Ishihara, T.; Tsujii, T.; Shudou, M.; Omokawa, Y.; et al. Temperature-Sensitive Nonionic Vesicles Prepared from Span 80 (Sorbitan Monooleate). *Langmuir* **2008**, *24*, 10762–10770. [[CrossRef](#)]
31. Shimanouchi, T.; Kawasaki, H.; Fuse, M.; Umakoshi, H.; Kuboi, R. Membrane fusion mediated by phospholipase C under endosomal pH conditions. *Colloids Surf. B* **2013**, *103*, 75–83. [[CrossRef](#)] [[PubMed](#)]

32. Klosgen, B.; Reichle, C.; Kohlsmann, S.; Kramer, K.D. Dielectric spectroscopy as a sensor of membrane headgroup mobility and hydration. *Biophys. J.* **1996**, *71*, 3251–3260. [[CrossRef](#)]
33. Sun, H.; Fan, L.; Zou, K.; Zhu, H.; Du, J. Decoration of homopolymer vesicles by antibacterial ultrafine silver nanoparticles. *RSC Adv.* **2014**, *4*, 41331–41335. [[CrossRef](#)]
34. van den Bogaart, G.; Guzman, J.V.; Mika, J.T.; Poolman, B. On the mechanism of pore formation by melittin. *J. Biol. Chem.* **2008**, *283*, 33854–33857. [[CrossRef](#)] [[PubMed](#)]
35. Nagasawa, D.; Azuma, T.; Noguchi, H.; Uosaki, K.; Takai, M. Role of Interfacial Water in Protein Adsorption onto Polymer Brushes as Studied by SFG Spectroscopy and QCM. *J. Phys. Chem. C* **2015**, *119*, 17193–17201. [[CrossRef](#)]
36. Ho, C.; Slater, S.J.; Stubbs, C.D. Hydration and order in lipid bilayers. *Biochemistry* **1995**, *34*, 6188–6195. [[CrossRef](#)]